Available online at www.sciencedirect.com
ScienceDirect
Solid State Ionics 179 (2008) 243–249
SOLID STATE IONICS
www.elsevier.com/locate/ssi

Nanostructured YSZ thin films for solid oxide fuel cells deposited by ultrasonic spray pyrolysis

M.F. García-Sánchez [a], J. Peña [a], A. Ortiz [a], G. Santana [a], J. Fandiño [b], M. Bizarro [a], F. Cruz-Gandarilla [c], J.C. Alonso [a,*]

[a] Instituto de Investigaciones en Materiales, Universidad Nacional Autónoma de México, Ciudad Universitaria, Coyoacán 04510, México D.F., México
[b] Universidad Autónoma de la Ciudad de México, Prolongación San Isidro 151, Iztapalapa 09790, México D.F., México
[c] Escuela Superior de Física y Matemáticas, IPN, Edif. 9, U.P.A.L.M., 07738, México D.F., México

Received 28 May 2007; received in revised form 26 September 2007; accepted 21 January 2008

Abstract

Nanostructured thin films of yttria-stabilized zirconia (YSZ) have been prepared on single-crystalline silicon substrates by ultrasonic spray pyrolysis using zirconium acetylacetonate and yttrium acetylacetonate hydrate as metallo-organic precursors dissolved in anhydrous methanol. The morphology, structure and electrical properties were studied by X-ray diffraction (XRD), scanning electron microscopy (SEM), atomic force microscopy (AFM) and impedance spectroscopy (IS). The substrate temperature was optimized for obtaining smooth, dense and homogeneous nanocrystalline films with grains sizes as small as 10 nm. The influence of thermal annealing on structural properties of films was studied. The activation energy measured for electrical conduction through the grains (1.14 eV) was similar to that obtained in bulk of YSZ, but for conduction through the grain boundaries it acquires a value of 0.79 eV, increasing the total conductivity of the material up to 0.033 S/cm at 650 °C. These activation energy values are related to the small grain size and the close boundaries obtained at the optimized conditions. The obtained films are good candidates for applications as electrolytes in solid oxide fuel cells (SOFC) operating at relatively low temperatures.

Keywords: YSZ; Nanostructure; Ultrasonic spray deposition

1. Introduction

Yttria-stabilized zirconia (YSZ) is commonly used as electrolyte material in solid oxide fuel cells (SOFC) and oxygen sensors due to its chemical and thermal stabilities, and its high oxygen ionic conductivity at high temperature [1–4]. However, in order to improve the performance of these devices, a lower operation temperature is desired. One approach to reduce this temperature is to increase the ionic conductivity of the YSZ electrolyte by decreasing its thickness as much as possible [5–9]. Some studies in this direction show that the ionic conductivity of YSZ can be enhanced by preparing cubic or tetragonal polycrystalline films with grain sizes in the nanometer range [8,9].

Several physical and chemical processes have been employed to prepare YSZ thin films, including pulsed laser ablation, electron-beam evaporation, sol–gel, polymeric precursor spin coating, spray pyrolysis in its three versions; electrostatic, pneumatic and ultrasonic, and others [6–25]. Among them, the spray pyrolysis techniques are very attractive for the industry of planar SOFCs, because they allow the deposition of a wide variety of ceramic films over large areas. Besides, they are probably the cheapest and simplest processes. Each one of the spray pyrolysis versions has advantages and drawbacks in terms of complexity and quality of deposit. Electrostatic spray deposition (ESD) has been widely used for preparing YSZ and other ZrO_2 based films [7,12–16]. This technique produce almost mono-dispersed and fine drops, however, the effect of preferential landing characteristic of the charged droplets can lead to porous and/or cracked films.

* Corresponding author. Tel.: +52 55 5622 4606; fax: +52 55 5616 1251.
E-mail address: alonso@servidor.unam.mx (J.C. Alonso).

0167-2738/$ - see front matter © 2008 Elsevier B.V. All rights reserved.
doi:10.1016/j.ssi.2008.01.088

Pressurized spray deposition is reported as a more adequate technique to deposit dense films compared to the ESD technique, however, there is less control on the microstructure of the deposited films due to a higher dispersion in droplet sizes [15]. Although in several papers an optimization of the ESD process parameters has been made to prepare dense YSZ films, their electrical properties were not reported in some of these cases [12–16]. Ultrasonic spray deposition (USD) allows a smaller and homogeneous droplet size than electrostatic or pressurized spray. This technique allows the deposition of homogeneous thin films with excellent physical properties [17]. USD using different solvents and precursors has been used for obtaining high quality ZrO_2 [18,19] and YSZ films [20–23]. For example, Matsuzaki et al. deposited thin films of YSZ using yttrium and zirconium octylates and substrate temperatures in the range from 873 to 1023 K. Although these YSZ films were dense, they have cubic crystalline structure with columnar growth and grains with sizes in the range from 73.5 to 265 nm. However, their electrical properties were not reported [20]. Beltrán et al. [22] used inorganic precursors and rapid thermal annealing at 900 °C to obtain crystalline YSZ films with cubic phase and activation energy for ionic conduction of 1.3 eV. Wang et al. [21] and Ramirez et al. [23] obtained better electrical properties in films deposited using yttrium and zirconium acetylacetonates at lower substrate temperatures (525–700 °C). In the former case the YSZ films deposited at 600 °C had a mixture of monoclinic and tetragonal crystalline phases with grain sizes from 80 to 120 nm, and the activation energy for ionic conduction was of 1.08 eV. In the latter case, YSZ film deposited at 525 °C had a cubic crystalline structure, with average grain size of ~22 nm and activation energy for ionic conduction of 1.0 eV. However, in both cases the effect of lower substrate temperatures on the microstructural and electrical properties of the films has not been investigated [21,23].

In the present work, ultrasonic spray deposition was used to deposit YSZ films at substrate temperatures lower than those previously used. In addition to ultrasonic mist, the influence of short distance of nozzle to substrate and a second gas injection zone in the nozzle was analyzed in order to improve the structural and electrical properties of the films. A study of the influence of temperature and deposition time on the morphology of the films was made. The electrical properties of the obtained films were measured and compared with previous reports.

2. Experimental

An experimental setup similar to that shown in reference [21] was used. However, in the present case the nozzle is equipped with a gas injection tube at the top of the nozzle (Fig. 1). This system allows to introduce a director gas for increasing or modifying the velocity of the droplets arriving on the heated substrate without altering the flow rate of the aerosol carrier gas. The diameter of the nozzle was 16 mm and the distance nozzle-substrate was fixed to 20 mm. Films were deposited onto (100) n-type, 200 Ω cm single-crystalline silicon slices in order to perform electrical measurements at high temperatures. The substrates were ultrasonically cleaned, with trichloroethylene, acetone, methanol and 5% HF solution in order to remove the native oxide. The spray solution was 0.025 M of zirconium (IV) acetylacetonate [$Zr(acac)_4 = Zr(C_5H_7O_2)_4$] from Sigma-Aldrich Chemicals and 0.01 M of yttrium acetylacetonate hydrate [$Y(acac)_3(H_2O)_x = Y(C_5H_7O_2)_3(H_2O)_x$], dissolved in anhydrous methanol. The carrier gas and director gas flow rates, air in both cases, were fixed at 3.5 l/min and 1.5 l/min, respectively. The temperature of the heating plate (Ts) was controlled in the range of 300–475 °C, and the deposition time (t_d) was varied between 5 and 25 min.

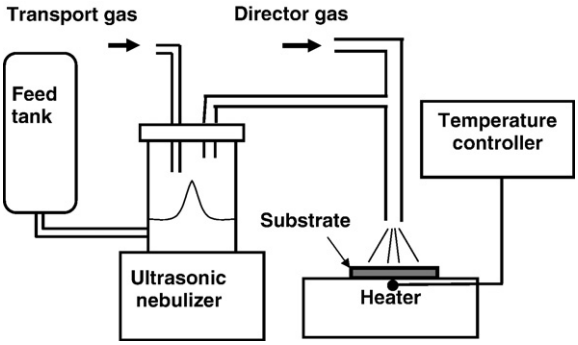

Fig. 1. Experimental setup used for ultrasonic spray deposition.

SEM images were obtained with a XL 30 FEG/SIRION with focused ion- and electron-beam, energy dispersive X-ray spectroscopy, and energy dispersive angle X-ray GENESIS 4000. An atomic force microscope (AFM) (Jeol, JSPM-4210) was used to analyze the surface of the samples. X-ray diffraction (XRD) spectra were obtained with a Siemens D-500 diffractometer using the CuK_α wavelength (1.54056 Å). The X-ray source was operated with a voltage of 25 kV and a current of 30 mA, to produce an intense X-ray beam whose incidence angle was 1°. The XRD spectra were obtained for 2θ angles in the range from 2° to 70° with steps of 0.020°. Considering the small thickness of the film, a long integration or step time (6.9 s) was used in order to obtain high quality XRD spectra. Under these experimental conditions the total acquisition time of each spectrum was around 11 h.

The thickness of the films was measured with a Sloan Dektac IIA profilometer. For this purpose a small part of the substrate was covered with a cover pyrex glass to form a step during deposition. The thickness of films was also measured by ellipsometry with a Gaertner 117A ellipsometer using the 633 nm line from a He–Ne laser. Both methods, ellipsometry and profilometry, gave similar thickness values for films deposited at the same conditions.

AC measurements were carried out using a Solartron 1260 Frequency Response Analyzer in combination with 1287 electrochemical interface over the range 0.1 Hz$<f<$32 MHz and for temperatures between 25 and 650 °C. A parallel pattern of two gold electrodes was sputtered on the film surface to be used as electrodes [21,26].

3. Results and discussion

Fig. 2a shows the dependence of the thickness of the film deposited at 425 °C as a function of deposition time. As can be

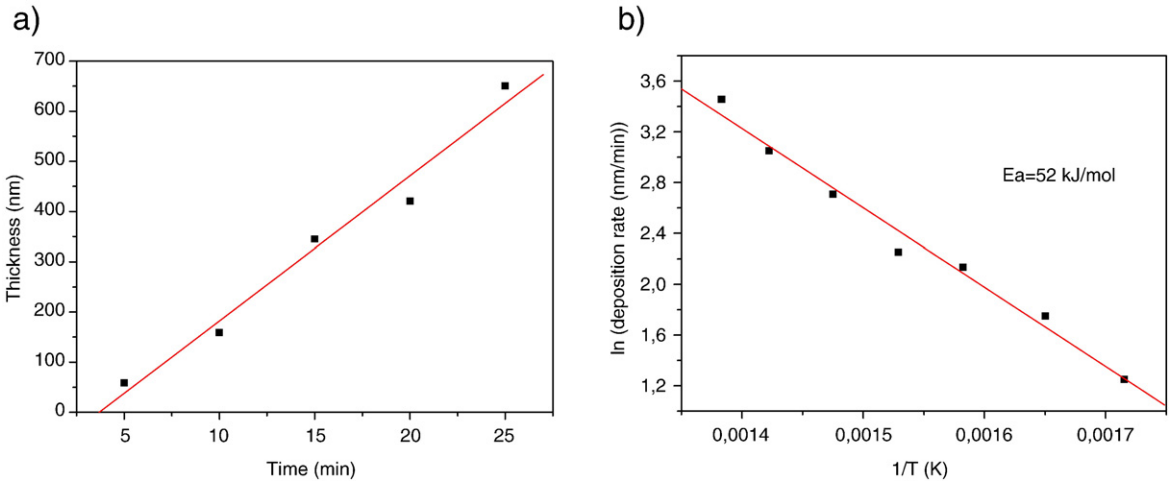

Fig. 2. a) Variation of thickness with deposition time and b) deposition rate as a function of substrate temperature.

seen, the thickness of the film increases linearly with the deposition time. A similar behavior was found for films deposited at the other substrate temperatures. The deposition rate, calculated from the slope of the best fitted straight line, increases as the substrate temperature increases. Fig. 2b shows a good linearity between the natural logarithm of deposition rate and the inverse of temperature for films deposited at temperatures between 310 and 450 °C. The activation energy of the growth rate obtained from the slope of the best-fit line in Fig. 2b is 52 kJ/mol. It is generally accepted that when the activation energy is greater than 42 kJ/mol, the deposition reaction is controlled by surface reactions [20]. Thus, the activation energy obtained in the present work can be related to a thermally activated deposition process in which the precursors decompose on reaching the growing film surface.

Typical SEM micrographs of the films grown during 10 min at 310, 400 and 475 °C are shown in Fig. 3a, b, and c, respectively. The films have good adherence to substrates, and no cracks or detachments were observed, even for films deposited at low temperatures. It must be due to the small

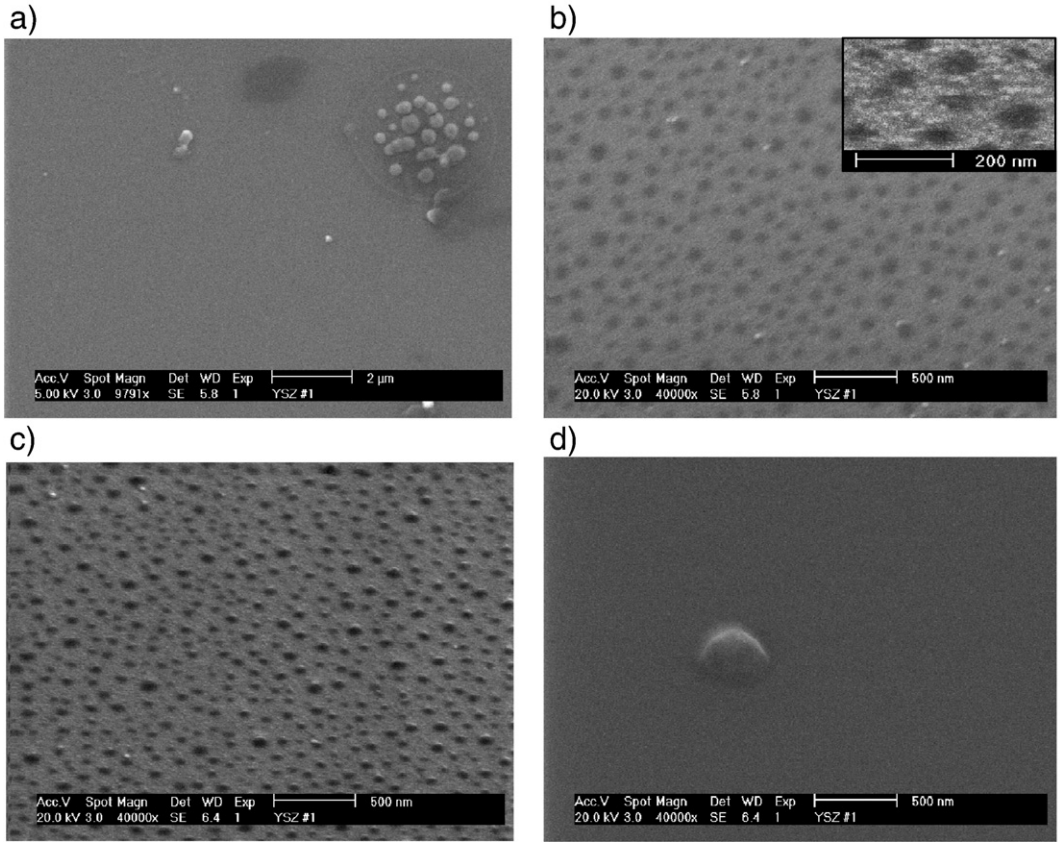

Fig. 3. SEM images of YSZ films grown at a) 310 °C for 10 min, b) 400 °C for 10 min, c) 475 °C for 10 min, d) 400 °C for 25 min.

droplet size and the small flow rate of the carrier gas, which allows the evaporation of solvents from droplets before arriving to the substrate, avoiding additional stresses during the fast drying process [24]. Moreover, taking into account that the temperature of substrate must be higher than the boiling temperature of the solvents [15], the use of methanol, with lower boiling temperature than that of the most used solvent butyl carbitol [6,12–16,24,27], is important in obtaining crack-free films at low substrate temperatures. This is a very important factor considering the potential application of these films in SOFC or oxygen sensor.

Fig. 3a shows that in samples deposited at the lowest substrate temperature (300 °C) can be observed splashes, forming more or less regular disk with a thin outer border. Inside the droplets there are trapped bubbles indicating that substrate temperature is not high enough to avoid that the solution boils on the surface of the substrate [16]. Then, the presence of splashes in the film is a clear indication that higher temperatures are necessary, as is described with details in reference 16. The splashes disappear with the increase of temperature.

In samples grown at 400 and 475 °C (Fig. 3b and c, respectively) similar microstructures were observed in SEM images. Dark zones were observed on surface of samples grown at substrate temperatures of 400 °C, or higher, for 10 min (Fig. 3b). During SEM observations, the samples were rotated so that it can be inferred that the dark zones were a consequence of a rolling surface, as is shown in Fig. 3c, but without pores in the films. The height of these undulations with reference to surface is of few nanometers. Increasing the magnification of SEM images, a nanostructured surface can be observed in samples grown at substrate temperatures higher to 400 °C (see inset in Fig. 3b). Using the Digital Micrograph software, the SEM images of these samples were analyzed and an average size of nanocrystals less to 10 nm was obtained.

The increase in deposition time does not produce important changes in morphology (cracks or roughness), but the dark zones are not present in samples grown at 400 °C (Fig. 3d). This suggests that the decomposition of precursors occurs after the droplet impacts on the surface of the substrate and a thin layer of liquid forms on the surface due to the fused precursors. This liquid layer may be responsible for the healing of surface defects observed in individual splats allowing a smooth surface [16]. We did not use too long deposition times as other reports [12–16,19,24,27,28] because it was not necessary to obtain films with thickness larger than 0.5 μm.

The low concentration of splashing residues at the surface of the film with respect to another report [12–16,24,26] is also a consequence of low substrate temperature and the low precursors concentration in the solution [16].

Considering that the decomposition temperature of $Zr(acac)_4$ and $Y(acac)_3$ is over 440 °C [21], a thermal annealing of the films was made at 500 °C. Although some changes should be expected with the total decomposition of organic precursors with the annealing (at least in films grown at 310 °C), the SEM results do not show any important change in the microstructure of the films (Fig. 4).

Fig. 5 shows the images obtained from AFM measurements for samples grown for 10 min with and without thermal annealing. At the lowest substrate temperature, the films have the prints of the droplets in their early states of spreading at the film surface [16]. This fact indicates that the temperature is too low, so that the droplets reach the heated substrate and there they form a liquid state before being decomposed into oxides (Fig. 5a), as was discussed in SEM measurements results (Fig. 3a). This film must be amorphous with residues of the precursors, which is undesirable. With the thermal annealing (Fig. 5b) some grains of less than 10 nm start to form in the film, but some nanopores also appear, which must be due to crystallization of the film and the total decomposition of the precursors. The small grain size could be the reason that clear differences can not be observed in SEM images.

The films grown at 400 °C show a homogeneous surface with grains of approximately 10 nm, without pores (Fig. 5c). The thermal annealing produces growing of the grain size [13], although without pores either (Fig. 5d). The fact that any important structural changes were observed with the thermal annealing indicates that this result is near to the optimal condition. That is, the solvent is evaporated while approaching the substrate surface, but the mist reaches the growing film surface, where the decomposition and chemical reaction

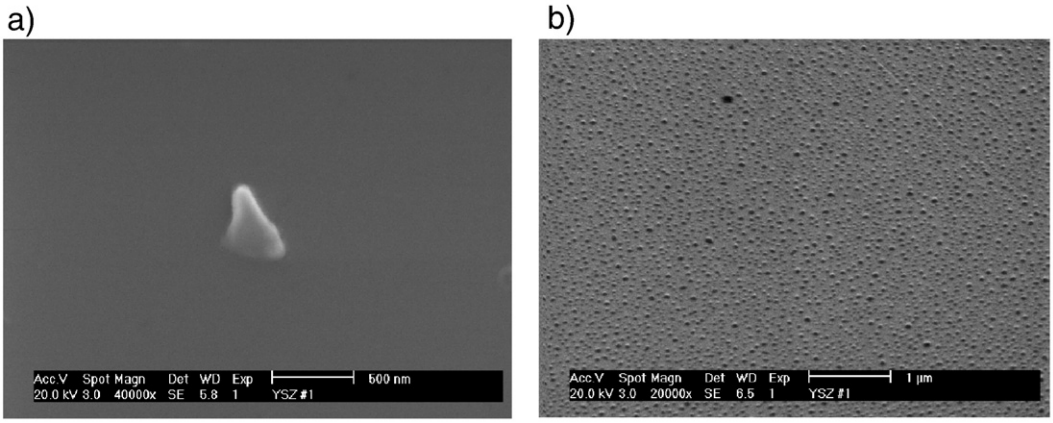

Fig. 4. SEM images of YSZ films grown at a) 310 °C and b) 400 °C for 10 min with a thermal annealing at 500 °C for 2 h.

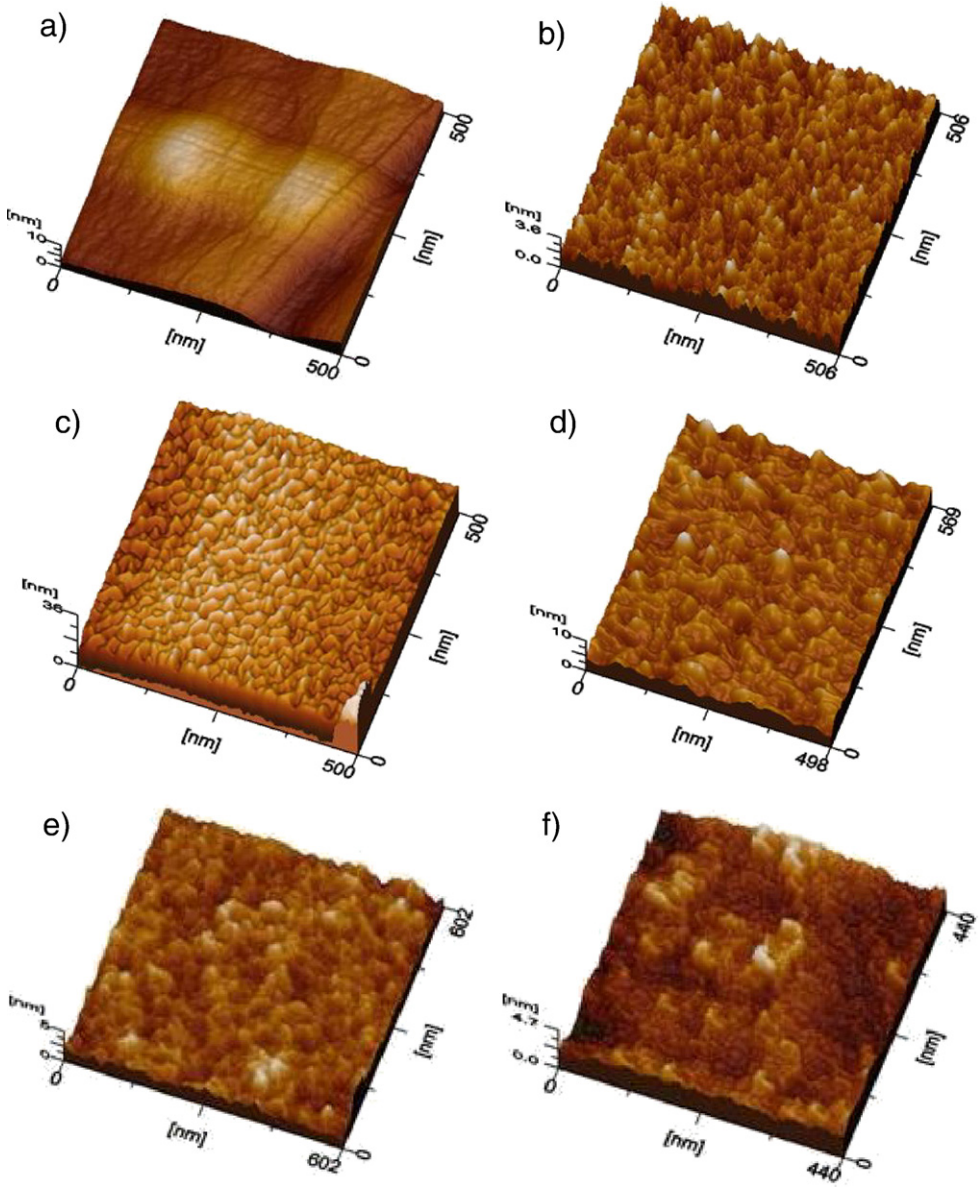

Fig. 5. AFM images of YSZ films grown for 10 min at a) 310 °C, b) 310 °C (TA), c) 400 °C, d) 400 °C (TA), e) 475 °C, f) 475 °C (TA); where (TA) indicates that samples were subjected to a thermal annealing.

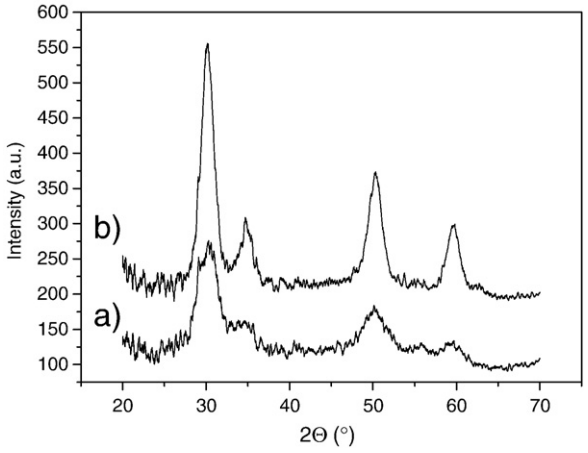

Fig. 6. XRD patterns of the film deposited at 400 °C a) without and b) with thermal annealing.

undergoes forming a dense thin film of YSZ [20,25]. This result is very important, as was commented, for applications of this material in SOFC.

The image of sample deposited at 475 °C shows a coral-like structure (Fig. 5e), which is indicative that dry material is impacting on the substrate. The increase of substrate temperature not only acts on its surface, but it also increases the droplets temperature while they are approaching to it. Due to the small

Table 1
Position of the four main XRD peaks and the determined cell parameters for analyzed samples, as well as the reported in Ref. [23]

Sample	1st peak	2nd peak	3rd peak	4th peak	*a* (Å)
Without TA	30.292		50.162	59.680	5.14
With TA	30.106	34.683	50.291	59.575	5.14
Ref. [23]	30.31	34.96	50.39	59.66	–

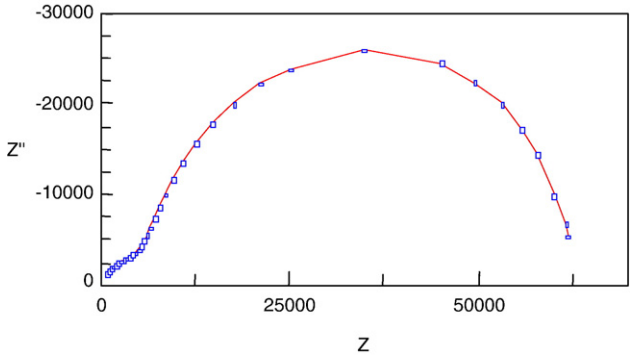

Fig. 7. Impedance response measured at 450 °C, for a sample grown at 425 °C.

droplets size and the low boiling point of the solvent, at 475 °C the droplets lose completely the solvent and the precursors begin to decompose before reaching the substrate. Consequently, the dry material simply adhere on the surface with no spreading, favouring the formation of a coral-like structure. The thermal annealing does not change appreciably the morphology of the film (Fig. 5f). These results indicate that chemical reaction and elimination of organic residues from precursors take place in the range between 400 °C and 475 °C, which is in agreement with previous reports [13].

Fig. 6 shows the results of DRX of a film grown at 400 °C. Before the thermal annealing three broad peaks can be observed (Fig. 6a), corresponding to a metastable cubic phase [19]. With the thermal annealing (Fig. 6b), more defined peaks appears, which could be attributed to either, the cubic and/or tetragonal phases since both exhibit diffraction peaks at nearly overlapping angles [21,23,24]. Given the yttria content and that the cubic phase is more stable at these temperatures [21,23], this phase was considered to make the analyses of the XRD spectra, although grain size effects must not be ruled out. In zirconia, with crystallite size below 30 nm, there exists either the metastable tetragonal phase at low temperature as result of the crystallite size effect [21,25], or amorphous material at sizes of few nanometers [29]. The partial crystallization in as-grown samples is in correspondence with the results discussed for AFM measurements.

Table 1 summarizes the position of the four main XRD peaks for analyzed samples, as well as those reported in Ref. [23]. Considering the relation between the peaks position and the content of yttrium [23], the ratio Y/Zr in the final composition is in concordance with the ratio in the precursor solution.

The average crystallite size was calculated from the Scherrer formula, corrected from the instrument contribution, for the (111) peak zirconia. The crystallite sizes in as-grown and annealed samples were of 8.4 and 9.5 nm, respectively, in agreement with the measured values by SEM. In this system setup the use of a low precursor concentration and an ultrasonic generated aerosol, allows to obtain small particle sizes [15]. The most important parameters for the film morphology are the substrate temperature and the initial droplet size. Firstly, the substrate temperature has to be above the boiling point of the solvent. Secondly, the initial droplets have to be large enough so they can reach the substrate without complete evaporation. The small particle size and the low gas flow rate allow the reduction of the distance to substrate [12,14]. The use of a short distance to substrate lead to a major deposition rate and the use of a second gas injection point allow the increase of the final gas flow rate without changing the carrier gas flow rate.

AC measurements were carried out from 25–650 °C for films grown at substrate temperature of 425 °C for 10 min (Fig. 7).

Two overlapping and little depressed semicircles were observed in the impedance complex plane plots (Fig. 7). This behavior is indicative of two processes which are associated with the electrolyte bulk (grain) and the grain boundary, in correspondence with previous reports [22,23,30,31]. The impedance diagrams were simulated, using the Zview program, by a series network of two sub-circuits, each one consisting of one resistor, and Constant Phase Element (CPE) and one capacitor in parallel. The CPE is incorporated to adjust the depression below the baseline of semicircles, typical in ionic conductors [32–34]. From this simulation, the total resistance,

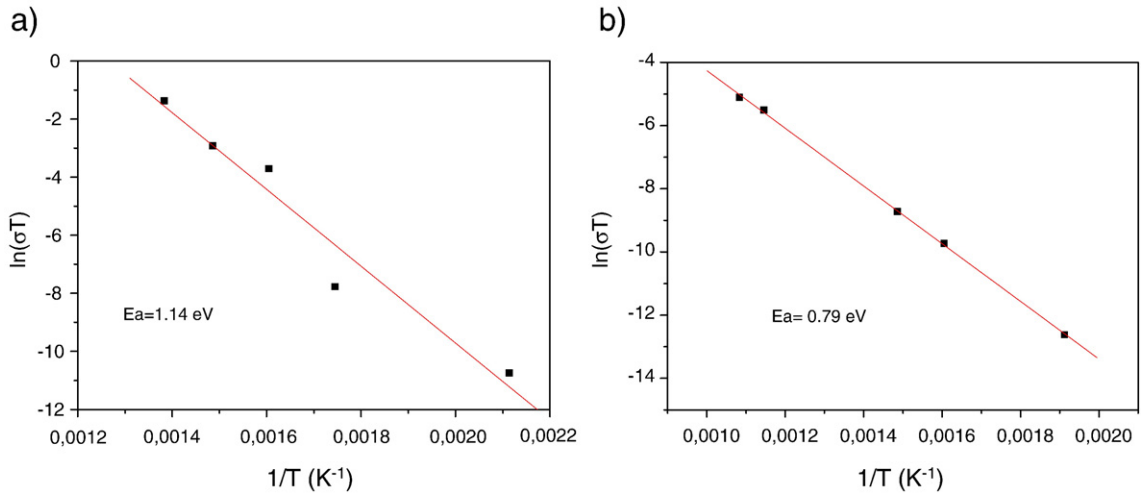

Fig. 8. Arrhenius ionic conductivity plots for a) grain and b) grain boundary.

R, was determined for each impedance diagram and then, the conductivity of each film as a function of temperature was calculated from the expression $\sigma = K/R$, where K is the geometric factor. The contribution of the Si substrate to the total resistance can be neglected because it is several orders of magnitude smaller.

The plot of log (σT) versus $1/T$ adjust quite well to straight lines (Fig. 8), which indicates that the conductivity for all these samples can be expressed in the form of the Arrhenius relationship: $\sigma T = A \exp(-\mathrm{Ea}/kT)$, where Ea is the activation energy for ion migration, A is the pre-exponential factor, k is the Boltzmann constant and T is the temperature in Kelvin.

The activation energy of grains (Fig. 8a) is in concordance with previous reports in bulk [4,8,10] and thin films [8,22,23,25,30,31]. This is an expected result because the activation energy is an intrinsic parameter of the material and it is supposed that not change with its way of preparation [8,33]. The activation energy of the grain boundary is slightly lower (Fig. 8b). In this case this value is related to concentration of defects in this zone and to the amount of contact points between the grains. The decrease of this parameter indicates that smooth boundaries were obtained with these experimental conditions. A total conductivity of 0.033 S/cm is obtained at 650 °C, which is better than that obtained at 800 °C by Jiang et al. [25] and is in correspondence with the results obtained by Kosacki et al. [8] in films with thickness of 50 nm obtained by pulsed laser ablation. This fact indicates that the conductivity of films is increased with the reduction of nanoparticles size, which is very important in low temperature electrochemical devices based in YSZ [8,9].

4. Conclusions

Smooth, dense and homogeneous YSZ films have been deposited in silicon substrates by ultrasonic spray pyrolysis. The use of ultrasonic generated mist and low concentration of precursor permitted to obtain small droplets. The decrease of droplet diameter allowed the use of low substrate temperature and short nozzle-substrate distance, increasing the deposition rate and reducing the splashing residues on the surface. Good adherence without cracks was obtained. With these experimental conditions nanostructured films with particles sizes smaller than 10 nm were obtained, which result in lower activation energy for conductivity through grain boundaries increasing the total conductivity of material.

Acknowledgements

The authors want to thank C. Flores, L. Baños, J. Camacho and S. Jimenez for technical assistance. This work has been partially supported by CONACyT—México, under project no. 47303-F and DGAPA–UNAM under project IN109803.

References

[1] N.Q. Minh, J. Am. Ceram. Soc. 76 (1993) 563.
[2] A.J. Appleby, J. Power Sources 69 (1996) 153.
[3] W.C. Maskell, Solid State Ionics 134 (2000) 43.
[4] R. Moreno, M.F. Garcia, G. Rodriguez, E. Perez-Cappe, Y. Echevarria, G. Perez, L. Ferrand, Quim. Anal. 18 (1999) 132.
[5] S. de Souza, S.J. Visco, L.C. De Jonghe, Solid State Ionics 98 (1997) 57.
[6] D. Perednis, L.J. Gauckler, Solid State Ionics 166 (2004) 229.
[7] J. Will, A. Mitterdorfer, C. Kleinlogel, D. Perednis, L.J. Gauckler, Solid State Ionics 131 (2000) 79.
[8] I. Kosacki, C.M. Rouleau, P.F. Becher, J. Bentley, D.H. Lowndes, Solid State Ionics 176 (2005) 1319.
[9] I. Kosacki, T. Suzuki, V. Petrovsky, H.U. Anderson, Solid State Ionics 136–137 (2000) 1225.
[10] M. Hartmanová, M. Jergel, V. Navrátil, K. Gmucová, F.C. Gandarilla, J. Zemek, Š. Chomik, F. Kundracik, Acta Phys. Slovaca 55 (2005) 247.
[11] H. Song, Ch. Xia, Y. Jiang, G. Meng, D. Peng, Mater. Lett. 57 (2003) 3833.
[12] R. Neagu, D. Perednis, A. Princivalle, E. Djurado, Solid State Ionics 177 (2006) 1981.
[13] R. Neagu, E. Djurado, L. Ortega, T. Pagnier, Solid State Ionics 177 (2006) 3491.
[14] R. Neagu, D. Perednis, A. Princivalle, E. Djurado, Surf. Coat. Technol. 200 (2006) 6815.
[15] O. Wilhelm, S.E. Pratsinis, D. Perednis, L.J. Gauckler, Thin Solid Films 479 (2005) 121.
[16] R. Neagu, D. Perednis, A. Princivalle, E. Djurado, Chem. Mater. 17 (2005) 902.
[17] M. Langlet, J.C. Joubert, in: C.N.R. Rao (Ed.), Chemistry of Advanced Materials, Blackwell Scientific Publications, Oxford, 1993, p. 55.
[18] A. Ortiz, J.C. Alonso, E. Haro-Poniatowski, J. Electron. Mater. 34 (2005) 150.
[19] H. Ruiz, H. Vesteghem, A.R. Di Giampaolo, J. Lira, Surf. Coat. Technol. 89 (1997) 77.
[20] Y. Matsuzaki, M. Hishinuma, I. Yasuda, Thin Solid Films 340 (1999) 72.
[21] H.B. Wang, C.R. Xia, G.Y. Meng, D.K. Peng, Mater. Lett. 44 (2000) 23.
[22] N.H. Beltrán, C. Balocchi, X. Errazu, R.E. Avila, G. Piderit, J. Electron. Mater. 27 (1998) 96.
[23] E.B. Ramírez, A. Huanosta, P.J. Sebastián, L. Huerta, A. Ortiz, J.C. Alonso, J. Mater. Sci. 42 (2007) 901.
[24] T. Nguyen, E. Djurado, Solid State Ionics 138 (2001) 191.
[25] Y. Jiang, J. Gao, M. Liu, Y. Wang, G. Meng, Solid State Ionics 177 (2007) 3405.
[26] A. Ramírez Duvergel, A.R. Ruiz Salvador, M.P. Hernández Sánchez, M.F. García Sánchez, G. Rodríguez Gattorno, Solid State Ionics 96 (1997) 89.
[27] D. Perednis, O. Wilhelm, S.E. Pratsinis, L.J. Gauckler, Thin Solid Films 474 (2005) 84.
[28] C.H. Chen, M.H.J. Emond, E.M. Kelder, B. Meester, J. Schoonman, J. Aerosol Sci. 30, 7 (1999) 959.
[29] M. Jouanne, J.F. Morhange, M.A. Kanehisa, E. Haro-Poniatowski, G.A. Fuentes, E. Torres, E. Hernández-Tellez, Phys. Rev. B 64 (2001) 155404.
[30] A. Rizea, G. Petot-Ervas, C. Petot, M. Abrudeanu, M.J. Graham, G.I. Sprule, Solid State Ionics 177 (2007) 3417.
[31] A.V. Chadwick, S.L.P. Savin, Solid State Ionics 177 (2006) 3001.
[32] M.F. García Sánchez, J.C. M´Peko, A.R. Ruiz Salvador, F. Fernández Gutierrez, G. Rodríguez Gattorno, A. Delgado, Y. Echevarría Inastrilla, J. Chem. Educ. 80 (9) (2003) 1062.
[33] M.-F. García-Sánchez, N. Fernández, M.-L. Martínez-Sarrión, L. Mestres, M. Herraiz, P. Escribano, E. Cordoncillo, H. Beltrán, Phys. Stat. Sol. B 242 (9) (2005) 1924.
[34] M.-L. Martínez-Sarrión, L. Mestres, M. Herráiz, O. Maqueda, N. Fernández, M.-F. García, Eur. J. Inorg. Chem. (2003) 2458.